Resource-Efficient Dissipative Entanglement of Two Trapped-Ion Qubits

Daniel C. Cole,[1,*] Stephen D. Erickson,[1,2] Giorgio Zarantonello,[1,2] Karl P. Horn,[3] Pan-Yu Hou,[1,2] Jenny J. Wu,[1,2] Daniel H. Slichter,[1] Florentin Reiter,[4] Christiane P. Koch,[3,5] and Dietrich Leibfried[1,†]

[1]*National Institute of Standards and Technology, 325 Broadway, Boulder, Colorado 80305, USA*
[2]*Department of Physics, University of Colorado, Boulder, Colorado 80309, USA*
[3]*Theoretische Physik, Universität Kassel, Heinrich-Plett-Straße 40, 34132 Kassel, Germany*
[4]*Institute for Quantum Electronics, ETH Zürich, Otto-Stern-Weg 1, 8093 Zürich, Switzerland*
[5]*Dahlem Center for Complex Quantum Systems and Fachbereich Physik, Freie Universität Berlin, Arnimallee 14, 14195 Berlin, Germany*

(Received 10 August 2021; accepted 2 December 2021; published 22 February 2022)

We demonstrate a simplified method for dissipative generation of an entangled state of two trapped-ion qubits. Our implementation produces its target state faster and with higher fidelity than previous demonstrations of dissipative entanglement generation and eliminates the need for auxiliary ions. The entangled singlet state is generated in ∼7 ms with a fidelity of 0.949(4). The dominant source of infidelity is photon scattering. We discuss this error source and strategies for its mitigation.

DOI: 10.1103/PhysRevLett.128.080502

Engineered dissipation has potential as a powerful tool for quantum applications [1,2]. Dissipation may be used for preparation of nonclassical states, including entangled states, and this approach can have reduced sensitivity to certain experimental imperfections and limitations [3,4]. Unlike unitary approaches, dissipative dynamics can produce target states from unknown or uncontrolled input states; examples in atomic physics include laser cooling and optical pumping. Some dissipative protocols can be implemented by continuous, stationary control fields, and can therefore continuously stabilize entangled states in the presence of noise. Numerous protocols for dissipative preparation of nonclassical states have been demonstrated [5–11], and more have been proposed [3,4,12–21]. Initial demonstrations [7,9] used strong driving to create resonances that were resolved and addressed by weaker drives [3,22,23]. These weaker drives could populate the target state without providing a path out of it in the limit where the timescales for the strong drive and the weaker drives were well separated. Recently, schemes have been explored that avoid these timescale hierarchies. Instead, they make more efficient use of experimental resources such as symmetries and auxiliary degrees of freedom [18–21,24,25], and are generally expected to produce target states faster and with higher fidelity.

Horn *et al.* have proposed a protocol for dissipative generation of an entangled singlet state $|S\rangle = (|\uparrow\downarrow\rangle - |\downarrow\uparrow\rangle)/\sqrt{2}$ of two trapped-ion qubits [19]. This scheme improves upon the demonstration in Ref. [7] by eliminating the timescale hierarchy and the need for sympathetic cooling, reducing the required number of ions from four to two. The protocol uses qubit levels $|\uparrow\rangle$ and $|\downarrow\rangle$, a stable auxiliary level $|\mathrm{aux}\rangle$, a short-lived excited state $|e\rangle$, and a mode of collective motion of the ions. Horn *et al.* applied quantum optimal control to explore the limits of this scheme, predicting singlet fidelities above 0.98 if heating of the motional mode used for the protocol could be kept low. An important fundamental source of heating is recoil of the ions after photon scattering. This heating rate is linked to the strengths of the interactions that generate the singlet state. In this Letter, we employ this protocol to generate an entangled singlet state with fidelity of 0.949(4), limited by photon scattering errors including recoil heating. We discuss how photon scattering limits the fidelity, theoretically investigate the large-Raman-detuning limit, and present strategies for improving the protocol's performance.

As shown in Fig. 1, the protocol involves simultaneous application of four global interactions, of which three are unitary: blue-sideband (anti-Jaynes-Cummings) couplings $|\downarrow, n\rangle \leftrightarrow |\uparrow, n+1\rangle$ and $|\mathrm{aux}, n\rangle \leftrightarrow |\uparrow, n+1\rangle$ driven by Hamiltonians H_{bq} and H_{ba}, respectively, and a qubit carrier transition $|\downarrow\rangle \leftrightarrow |\uparrow\rangle$ driven by Hamiltonian H_c. The states $|n\rangle$ are number states of the motional degree of freedom with creation operator $a^\dagger$. The Hamiltonians are:

$$H_{bq} = \frac{\hbar\Omega_{bq}}{2} a^\dagger (|\uparrow\rangle_1\langle\downarrow|_1 + |\uparrow\rangle_2\langle\downarrow|_2) + \mathrm{H.c.}, \quad (1)$$

$$H_{ba} = \frac{\hbar\Omega_{ba}}{2} a^\dagger (|\uparrow\rangle_1\langle\mathrm{aux}|_1 + |\uparrow\rangle_2\langle\mathrm{aux}|_2) + \mathrm{H.c.}, \quad (2)$$

$$H_c = \frac{\hbar\Omega_c}{2} (|\uparrow\rangle_1\langle\downarrow|_1 + |\uparrow\rangle_2\langle\downarrow|_2) + \mathrm{H.c.}, \quad (3)$$

where H_c implements the identity on the motion, the subscripts 1 and 2 label the ions, and Ω_I denotes the

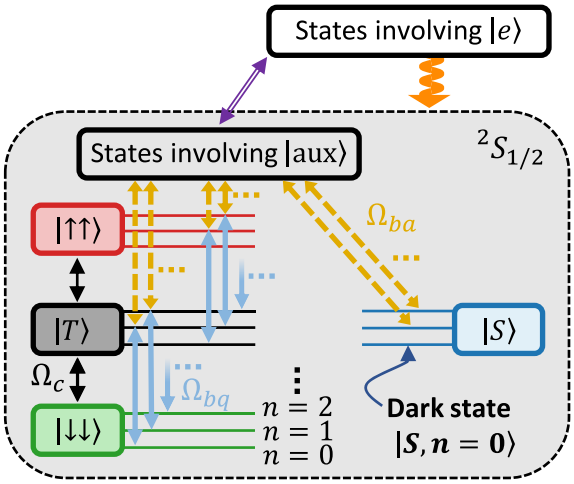

FIG. 1. Protocol for dissipative singlet generation. Four interactions combine to generate the joint state $|S, n = 0\rangle$ of two ions and their collective motion. Blue-sideband transitions are depicted by solid blue (H_{bq}) and dashed yellow (H_{ba}) arrows, and a qubit carrier interaction (implementing the identity on the motion) is depicted by thin black arrows. This carrier interaction depopulates the $|\uparrow\uparrow, n = 0\rangle$ state, which is otherwise dark. Excitation of $|\text{aux}\rangle$ to $|e\rangle$ and decay back to the ground state are shown by the double purple and snaking orange arrows, respectively. Next to each qubit state are several rungs of the motional number state ladder, and ellipses indicate continuation of interactions to higher states. No path exists out of the state $|S, n = 0\rangle$, which is populated by decay from states involving $|e\rangle$.

Rabi frequency of interaction H_I. The fourth, dissipative interaction is effective decay from $|\text{aux}\rangle$ back to $|\uparrow\rangle$, $|\downarrow\rangle$, and $|\text{aux}\rangle$, which is engineered via excitation to and decay from $|e\rangle$.

As depicted in Fig. 1, the interactions H_{bq} and H_c couple the states $|\downarrow\downarrow\rangle$, $|T\rangle = (|\uparrow\downarrow\rangle + |\downarrow\uparrow\rangle)/\sqrt{2}$, and $|\uparrow\uparrow\rangle$ within the total-spin-1 qubit manifold and, together with H_{ba}, provide a path for one of the qubits to transition to $|\text{aux}\rangle$ when starting in any of these states, regardless of the initial motional occupation n. Dissipative pumping out of $|\text{aux}\rangle$ continuously reshuffles population until it arrives in the state $|S, n = 0\rangle$. Population becomes trapped there because $|S\rangle$ is invariant under the qubit interactions H_c and H_{bq}, and coupling of the $|\uparrow\rangle$ component of $|S\rangle$ to $|\text{aux}\rangle$ due to H_{ba} only occurs when $n > 0$. Neglecting errors and imperfections, the theoretical steady-state fidelity for generation of $|S, n = 0\rangle$ is unity.

We realize this protocol with two $^9Be^+$ ions trapped along the axis of a linear Paul trap [26]. A combination of static and rf electric potentials at 82.5 MHz applied to the trap electrodes confines the ions such that they have an equilibrium axial separation of 3.7 μm and exhibit quantized collective motion in three dimensions. The frequencies for the in-phase and out-of-phase ("stretch") axial motional modes are 4 MHz and $f_s = 7$ MHz, respectively, and the stretch mode is used to engineer the entanglement.

We apply an 11.9 mT magnetic quantization field [27] and identify the levels $|\downarrow\rangle$, $|\uparrow\rangle$, and $|\text{aux}\rangle$ with Zeeman sublevels of the $^9Be^+$ $^2S_{1/2}$ ground state labeled by hyperfine and magnetic quantum numbers F and m_F: $|\downarrow\rangle = |F = 2, m_F = 2\rangle$, $|\uparrow\rangle = |1, 1\rangle$, and $|\text{aux}\rangle = |2, 1\rangle$. The Hamiltonian H_c is realized using microwave radiation with frequency near 1.018 GHz from an external antenna, and the Hamiltonians H_{bq} and H_{ba} are realized by driving stimulated-Raman transitions with 313 nm laser radiation tuned hundreds of gigahertz below the $^2S_{1/2} \leftrightarrow {}^2P_{1/2}$ transition. The beam geometry is depicted in Fig. 2(a).

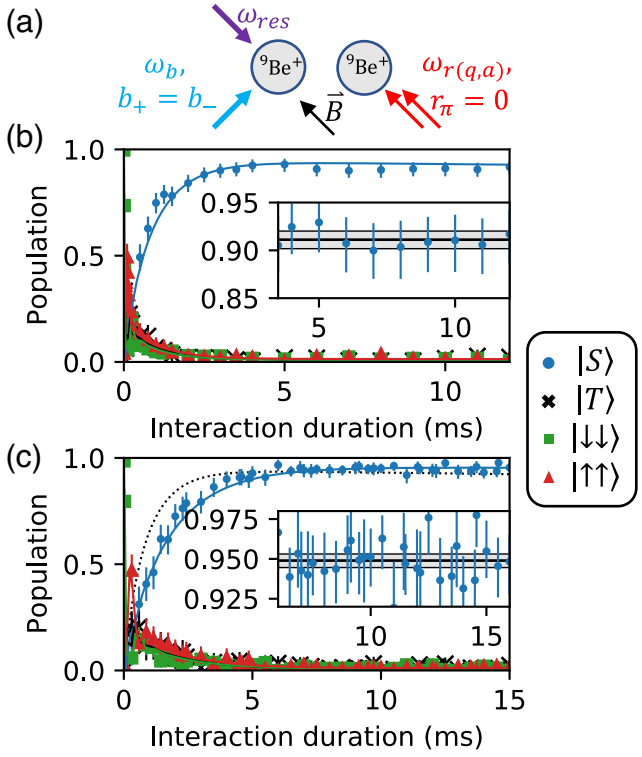

FIG. 2. Experimental geometry and results. (a) Ions, magnetic field, and $\vec{k}$ vectors for four laser beams: higher-frequency Raman beam (blue), copropagating lower-frequency Raman beams at frequencies ω_{rq} and ω_{ra} (red), and a resonant beam with variable frequency ω_{res} that drives either the $|\text{aux}\rangle \leftrightarrow |e\rangle$ coupling or the cycling transition. Beams have 25 μm waists and illuminate both ions approximately equally. Constraints on the polarizations of the Raman beams, as indicated next to the $\vec{k}$ vectors by components $(b/r)_{\pm,\pi}$ (see text), arise due to their orientations relative to the quantization field. (b),(c) Measured populations in four basis states as a function of interaction duration for Raman detunings of -315 GHz (b) and -450 GHz (c). Solid lines are simulations with no free parameters. For -315 GHz detuning, the simulation includes a ϕ error of 0.05 rad (see text) and uses the measured $|\text{aux}\rangle$ depletion time of 34 μs. The simulated singlet curve from (b) is replicated in (c) as a dotted black line for comparison. Insets show data on the fidelity plateau. Horizontal black lines and shading indicate the average fidelity on the plateau and a 95% confidence interval. Error bars indicate 95% confidence intervals on individual points.

The Raman transitions are driven on the blue sideband corresponding to excitation of the axial stretch mode. This mode is chosen for its relatively low heating rate due to its reduced sensitivity to homogeneous electric fields, which arises because the mode eigenvectors for the two ions are exact opposites [28]. A 313 nm $\hat{\sigma}_+$-polarized repump laser resonantly couples $|\mathrm{aux}\rangle$ to $|e\rangle = |^2P_{1/2}, F = 2, m_F = 2\rangle$, which decays at a rate $\Gamma \approx 2\pi \times 20$ MHz back to $|\uparrow\rangle$, $|\downarrow\rangle$, and $|\mathrm{aux}\rangle$ with approximate branching ratio 5:4:3 [7]. Angular momentum conservation dictates that $|e\rangle$ decays only to these three states, and other transitions that may be driven by the same laser are far off resonant.

The microwave field, with wavelength $\lambda_{\mu w} \gg |\vec{r}_1 - \vec{r}_2| = 3.7\,\mu$m, is nearly the same at the positions $\vec{r}_1$ and $\vec{r}_2$ of the two ions. In the interaction picture for the qubit levels, the microwave Hamiltonian can be written in the form given by Eq. (3). This defines a relationship between the orientations of the two qubits' Bloch spheres. The qubit sideband interaction then implements the experimental interaction-picture Hamiltonian $H_{bq}^{(e)}$ [21,29]:

$$\begin{aligned} H_{bq}^{(e)} &= \frac{\hbar\Omega_{bq}}{2} a^\dagger (e^{i(\Delta\vec{k}\cdot\vec{r}_1+\theta)}|\uparrow\rangle_1\langle\downarrow|_1 \\ &\quad - e^{i(\Delta\vec{k}\cdot\vec{r}_2+\theta)}|\uparrow\rangle_2\langle\downarrow|_2) + \mathrm{H.c.} \\ &= e^{i\Phi}\frac{\hbar\Omega_{bq}}{2} a^\dagger (|\uparrow\rangle_1\langle\downarrow|_1 - e^{i\phi}|\uparrow\rangle_2\langle\downarrow|_2) + \mathrm{H.c.} \end{aligned} \tag{4}$$

Here $\Delta\vec{k}$ is the difference wave vector between the Raman beams, and the sign difference arises because the two ions move in opposite directions in the stretch mode. We have introduced the phases $\phi = \Delta\vec{k}\cdot(\vec{r}_2 - \vec{r}_1)$ and $\Phi = \Delta\vec{k}\cdot\vec{r}_1 + \theta$, where θ is a reference phase for the interference pattern between the two Raman beams that fluctuates due to lack of interferometric stability between the beams. When ϕ is set to π [see Supplemental Material (SM) [30]], $H_{bq}^{(e)}$ coincides with H_{bq} up to the fluctuating rotation axis defined by Φ. These fluctuations have negligible effect on generation or invariance of the singlet because they are slow relative to the entanglement dynamics [34].

To implement two stimulated-Raman sideband transitions simultaneously, we apply far-detuned laser light at three frequencies ω_b (higher frequency "blue" beam) and $\omega_{r(q,a)}$ ("red" beams, with subscripts denoting the corresponding Hamiltonian) with frequency differences $\omega_b - \omega_{rq} = (E_\uparrow - E_\downarrow)/\hbar + 2\pi f_s$ and $\omega_b - \omega_{ra} = (E_\uparrow - E_{\mathrm{aux}})/\hbar + 2\pi f_s$, where E_j is the energy of state j. In this three-frequency configuration $\omega_{rq} - \omega_{ra} = (E_\downarrow - E_{\mathrm{aux}})/\hbar$, so the two red beams can resonantly drive stimulated-Raman $|\downarrow\rangle \leftrightarrow |\mathrm{aux}\rangle$ carrier transitions. This would depopulate the singlet state. However, the red beams' $\vec{k}$ vector is approximately parallel to the quantization field. Therefore, the component r_π of the red beams' polarization unit vector (r_-, r_π, r_+), with entries corresponding to $\hat{\sigma}_-$, $\hat{\pi}$, and $\hat{\sigma}_+$ polarizations, is $r_\pi \approx 0$. The Rabi frequency of the $|\downarrow\rangle \leftrightarrow |\mathrm{aux}\rangle$ coupling is proportional to this component, so the coupling is suppressed.

We implement this singlet generation protocol and investigate its performance. Simulations indicate that the system can be initialized in any mixture of states in which each ion is in $|\uparrow\rangle$, $|\downarrow\rangle$, or $|\mathrm{aux}\rangle$ and n is not too large [30]. We begin by approximately preparing $|\downarrow\downarrow, n = 0\rangle$ with optical pumping, Doppler cooling, and sideband cooling. We then simultaneously apply the four interactions for a variable duration t. Finally, we measure the populations in four 2-qubit basis states by performing global rotations on the qubits and then performing fluorescence detection on the $|\downarrow\rangle \leftrightarrow |^2P_{3/2}, F = 3, m_F = 3\rangle$ cycling transition. From the photon count histograms for each condition, maximum-likelihood estimates are obtained for populations $P_{n,A}(t)$ with n ions in the bright $|\downarrow\rangle$ state under analysis condition A. We use three analysis conditions: no rotation, π pulse, and $\pi/2$ pulse with randomized phase. These yield populations $P_{n,I}$, $P_{n,\pi}$, and $P_{n,\pi/2}$, respectively. Basis-state populations are then obtained as [7]:

$$P_{\downarrow\downarrow} = P_{2,I}, \tag{5}$$

$$P_{\uparrow\uparrow} = P_{2,\pi}, \tag{6}$$

$$P_S - P_{ll} \equiv X = 1 - 2P_{0,\pi/2} - (P_{2,I} + P_{2,\pi})/2, \tag{7}$$

$$P_T = 2P_{2,\pi/2} - (P_{2,I} + P_{2,\pi})/2. \tag{8}$$

The singlet population exceeds X by the population P_{ll} ("leakage-leakage") with both ions in states other than $\{|\uparrow\rangle, |\downarrow\rangle\}$, but this is small and $P_S \approx X$ in practice.

We investigate singlet generation for two detunings $\nu_{\mathrm{laser}} - \nu_{\mathrm{ion}}$ of the Raman beams, with frequencies approximately ν_{laser}, from the $^2S_{1/2} \leftrightarrow {}^2P_{1/2}$ transition with frequency ν_{ion}. The importance of this detuning is described below. We show the results in Figs. 2(b) and 2(c). We plot measured populations obtained from Eqs. (5)–(8), with uncertainties determined by bootstrapping. In the inset of each figure we show the data on a pseudo-steady-state fidelity plateau and a confidence interval (CI) for the plateau fidelity. This CI and the plotted uncertainties are bias-corrected 95% bootstrap CIs [35]. For −315 GHz detuning we measure a fidelity (CI) of 0.911 ([0.902, 0.920]), and for −450 GHz we measure 0.949 ([0.945, 0.953]). We describe the bootstrapping procedure in the SM [30].

Figures 2(b) and 2(c) also show simulations of the dynamics. The simulations use the measured Rabi frequencies of the unitary interactions, the $|\mathrm{aux}\rangle$ repumping time constant, the Lamb-Dicke parameter for the stretch mode, and the Stark shifts induced by the Raman lasers, all determined in separate measurements. The simulations

incorporate spontaneous Raman and Rayleigh scattering driven by the Raman lasers [36] and recoil associated with scattering Raman and repump photons. They also include a unitary coupling between $|\downarrow\rangle$ and $|\mathrm{aux}\rangle$ arising from a residual nonzero $\hat{\pi}$-polarization component r_π of the red Raman beams [30]. The peak fidelity predicted by the simulation for −450 GHz detuning is 0.954, consistent with the upper CI bound of 0.953 for the average fidelity between 6 and 16 ms. For −315 GHz detuning the predicted peak fidelity is 0.946, lower than for −450 GHz due to larger scattering error. Including a typical calibration error of 0.05 rad for the phase ϕ in Eq. (4) reduces the peak fidelity to 0.935. Using an $|\mathrm{aux}\rangle$ repumping time constant of 51 μs instead of the measured 34 μs reduces the peak to 0.912, consistent with the measurement. The repumper amplitude is not stabilized during the experiment and is known to drift. We hypothesize that the cause of the difference between the measurements and simulations is these and similar errors. Other explanations, including that our model is incomplete, are possible. We present simulation details in the SM [30].

This singlet-generation protocol is robust against some typical experimental errors, including magnetic field fluctuations and laser phase noise. However, the scheme is sensitive to differential effects between the two ions, including differences in the Rabi frequencies of the qubit transitions and differential qubit frequency shifts (caused by, e.g., magnetic field gradients and differential ac Stark shifts). In our implementation, we have made errors from these differential effects negligible. This is demonstrated by direct measurements of the size of these effects [30] and also by the agreement of the model with the data. For −315 GHz (−450 GHz) Raman detuning we calculate an infidelity contribution of 0.008 (0.009) from residual $|\downarrow\rangle \leftrightarrow |\mathrm{aux}\rangle$ coupling. Calibration errors likely contribute to the infidelity for −315 GHz detuning as described above. In both cases, the remaining infidelity is due to undesired photon scattering.

Figure 3(a) show the relevant scattering processes. Spontaneous Raman transitions between $|\uparrow\rangle$, $|\downarrow\rangle$, and $|\mathrm{aux}\rangle$ can be corrected by the singlet-generation dynamics and so do not accumulate, but instead decrease the steady-state fidelity. Transitions to other states lead to permanent (to first order) population loss and fidelity decay. In principle, Rayleigh scattering has two effects. First, Rayleigh scattering can cause decoherence of the qubit. The decoherence rate is related to the differences between the scattering amplitudes off of the two states for each polarization [19,37]. However, the singlet is in a decoherence-free subspace [27,38–40], so differential decoherence between the two ions is required to affect the singlet fidelity. This occurs only to the extent that the environment resolves which of the ions scattered a photon [41]. By following reasoning similar to that in Ref. [37], we estimate an upper bound of 1.5×10^{-4} for the factor by

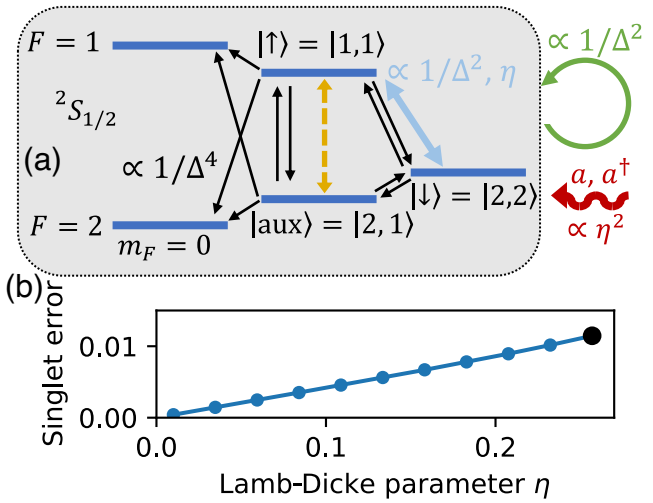

FIG. 3. Photon scattering error in singlet generation. (a) Scattering processes include stimulated-Raman sideband transitions (thick light blue arrow and dashed yellow arrow), spontaneous Raman transitions (thin black arrows), and Rayleigh scattering (green loop indicating the identity operation on the ions' internal state). These processes asymptotically scale with the detuning as $1/\Delta^2$, $1/\Delta^4$, and $1/\Delta^2$, respectively. Recoil leads to heating (modeled by jump operators proportional to products of a and $a^\dagger$ and indicated by the snaking red arrow) at a rate proportional to η^2 to leading order, where η is the Lamb-Dicke parameter. (b) A calculation of the infidelity as a function of η in the large-detuning limit; increasing the strength of the confining potential and therefore decreasing η improves the performance. The larger black dot indicates the value $\eta = 0.257$ used in the experiment.

which differential decoherence is suppressed relative to single-ion decoherence, so we neglect this differential Rayleigh decoherence in our model for the experiment. The second effect of Rayleigh scattering is recoil heating. This heating provides a path out of the target $|S, n = 0\rangle$ state, and is included in our model as an important error source.

Photon scattering error can be reduced at the cost of increased singlet preparation time. Limitations on this approach come from restrictions on the preparation time and timescales at which other errors become relevant. The error from spontaneous Raman transitions can be reduced by increasing the Raman detuning Δ, because the asymptotic scalings of the rates for stimulated and spontaneous Raman scattering are $1/\Delta^2$ and $1/\Delta^4$, respectively. Therefore, $|\Delta|$ should be as large as is practical. In the large-detuning limit $|\Delta| \to \infty$, the only remaining error source is recoil heating from Rayleigh scattering (neglecting differential Rayleigh decoherence). We investigate the protocol's performance in this limit by optimizing the laser polarizations and interaction strengths [30]. For the Lamb-Dicke parameter $\eta = 0.257$ used in the experiment, we calculate a fidelity of 0.989 and optimal [respecting the constraints shown in Fig. 2(a)] Raman beam polarizations

of blue-beam $\hat{\pi}$ component $b_\pi = 0.59$ and red-beam $\hat{\sigma}_+$ component $r_+ = 0.88$. These are close to the experimental polarizations $b_\pi = 0.62$, $r_+ \approx 1$, chosen to be near-optimal and experimentally convenient.

The stimulated-Raman sideband Rabi rate scales as η while the recoil heating rate scales as η^2, so the error for large detuning can be reduced by decreasing η. We numerically investigate the dependence of the large-detuning steady-state singlet fidelity on η and present the results in Fig. 3(b). The error decreases linearly with η and falls below 0.01 (0.001) at $\eta = 0.229$ (0.024). The time to approach the asymptotic fidelity scales as $1/\eta$ due to the reduced Rabi rates for the stimulated-Raman sideband transitions.

The fidelity may also be improved by incorporating sympathetic cooling. Periods of cooling should alternate with the singlet-generation dynamics to avoid interfering with the coupling $|\downarrow, n=0\rangle \leftrightarrow |\uparrow, n=1\rangle \leftrightarrow |\mathrm{aux}, n=0\rangle$. We find in simulations that if the stretch mode is reinitialized to $n = 0$ after each period $2\pi/\Omega_{ba}$ of the H_{ba} coupling, then the large-detuning-limit fidelity increases to 0.994. However, without cooling the simulated steady-state motional occupation of the singlet is $\bar{n} = 0.002$. Ground-state cooling performance to at least this level would be required to improve the fidelity, so this strategy may be difficult to productively implement in practice. Finally, the performance could be improved by driving the sidebands not with lasers but with magnetic field gradients [42–46]. These interactions typically have smaller sideband Rabi frequencies and would therefore have slower entanglement dynamics, but could make photon scattering error negligible.

Our demonstration of dissipative singlet generation with fidelity of 0.949(4), along with related work by Malinowski *et al.* [24], advances the dissipative production of entangled resource states. These works indicate a path toward fidelities that could allow productive incorporation of dissipative protocols into practical trapped-ion platforms for quantum applications. In this work, the success of the photon scattering model indicates that numerical simulations can be a powerful tool for optimizing trapped-ion dissipative protocols and supports our conclusion that the current limitation on fidelity arises from photon scattering errors. We have further investigated the role of these errors in entanglement generation, which has been considered in depth for unitary approaches [36] and represents an outstanding challenge for the realization of practical trapped-ion quantum computers [47].

The authors thank Ethan Clements and Shawn Geller for comments on the manuscript and Emanuel Knill and Scott Glancy for helpful discussions. This work was supported by IARPA and the NIST Quantum Information Program. D. C. C. acknowledges support from a National Research Council postdoctoral fellowship. S. D. E. acknowledges support from the National Science Foundation under Grant No. DGE 1650115. P.-Y. H and J. J. W. acknowledge support from the Professional Research Experience Program (PREP) operated jointly by NIST and University of Colorado Boulder. F. R. acknowledges financial support from the Swiss National Science Foundation (Ambizione Grant No. PZ00P2_186040). K. P. H. and C. P. K. acknowledge financial support from the Federal State of Hesse, Germany, through the SMolBits project within the LOEWE program and from the DFG Collaborative Research Center (CRC) 183 Grant No. 277101999—project B02.

*Present address: ColdQuanta, Inc., 3030 Sterling Circle, Boulder, Colorado 80301, USA.
†dietrich.leibfried@nist.gov

[1] J. F. Poyatos, J. I. Cirac, and P. Zoller, Quantum Reservoir Engineering with Laser Cooled Trapped Ions, Phys. Rev. Lett. **77**, 4728 (1996).
[2] F. Verstraete, M. M. Wolf, and J. Ignacio Cirac, Quantum computation and quantum-state engineering driven by dissipation, Nat. Phys. **5**, 633 (2009).
[3] M. J. Kastoryano, F. Reiter, and A. S. Sørensen, Dissipative Preparation of Entanglement in Optical Cavities, Phys. Rev. Lett. **106**, 090502 (2011).
[4] G. Morigi, J. Eschner, C. Cormick, Y. Lin, D. Leibfried, and D. J. Wineland, Dissipative Quantum Control of a Spin Chain, Phys. Rev. Lett. **115**, 200502 (2015).
[5] H. Krauter, C. A. Muschik, K. Jensen, W. Wasilewski, J. M. Petersen, J. I. Cirac, and E. S. Polzik, Entanglement Generated by Dissipation and Steady State Entanglement of Two Macroscopic Objects, Phys. Rev. Lett. **107**, 080503 (2011).
[6] J. T. Barreiro, M. Müller, P. Schindler, D. Nigg, T. Monz, M. Chwalla, M. Hennrich, C. F. Roos, P. Zoller, and R. Blatt, An open-system quantum simulator with trapped ions, Nature (London) **470**, 486 (2011).
[7] Y. Lin, J. P. Gaebler, F. Reiter, T. R. Tan, R. Bowler, A. S. Sørensen, D. Leibfried, and D. J. Wineland, Dissipative production of a maximally entangled steady state of two quantum bits, Nature (London) **504**, 415 (2013).
[8] D. Kienzler, H.-Y. Lo, B. Keitch, L. de Clercq, F. Leupold, F. Lindenfelser, M. Marinelli, V. Negnevitsky, and J. P. Home, Quantum harmonic oscillator state synthesis by reservoir engineering, Science **347**, 53 (2015).
[9] S. Shankar, M. Hatridge, Z. Leghtas, K. M. Sliwa, A. Narla, U. Vool, S. M. Girvin, L. Frunzio, M. Mirrahimi, and M. H. Devoret, Autonomously stabilized entanglement between two superconducting quantum bits, Nature (London) **504**, 419 (2013).
[10] M. E. Kimchi-Schwartz, L. Martin, E. Flurin, C. Aron, M. Kulkarni, H. E. Tureci, and I. Siddiqi, Stabilizing Entanglement via Symmetry-Selective Bath Engineering in Superconducting Qubits, Phys. Rev. Lett. **116**, 240503 (2016).
[11] Y. Liu, S. Shankar, N. Ofek, M. Hatridge, A. Narla, K. M. Sliwa, L. Frunzio, R. J. Schoelkopf, and M. H. Devoret, Comparing and Combining Measurement-Based and Driven-Dissipative Entanglement Stabilization, Phys. Rev. X **6**, 011022 (2016).

[12] M. B. Plenio, S. F. Huelga, A. Beige, and P. L. Knight, Cavity-loss-induced generation of entangled atoms, Phys. Rev. A **59**, 2468 (1999).
[13] A. W. Carr and M. Saffman, Preparation of Entangled and Antiferromagnetic States by Dissipative Rydberg Pumping, Phys. Rev. Lett. **111**, 033607 (2013).
[14] D. D. Bhaktavatsala Rao and K. Mølmer, Dark Entangled Steady States of Interacting Rydberg Atoms, Phys. Rev. Lett. **111**, 033606 (2013).
[15] F. Ticozzi and L. Viola, Steady-state entanglement by engineered quasi-local Markovian dissipation, Quantum Inf. Comput. **14**, 265 (2014).
[16] F. Reiter, D. Reeb, and A. S. Sørensen, Scalable Dissipative Preparation of Many-Body Entanglement, Phys. Rev. Lett. **117**, 040501 (2016).
[17] X. Q. Shao, J. H. Wu, X. X. Yi, and G.-l. Long, Dissipative preparation of steady Greenberger-Horne-Zeilinger states for Rydberg atoms with quantum Zeno dynamics, Phys. Rev. A **96**, 062315 (2017).
[18] C. D. B. Bentley, A. R. R. Carvalho, D. Kielpinski, and J. J. Hope, Detection-Enhanced Steady State Entanglement with Ions, Phys. Rev. Lett. **113**, 040501 (2014).
[19] K. P. Horn, F. Reiter, Y. Lin, D. Leibfried, and C. P. Koch, Quantum optimal control of the dissipative production of a maximally entangled state, New J. Phys. **20**, 123010 (2018).
[20] E. Doucet, F. Reiter, L. Ranzani, and A. Kamal, High fidelity dissipation engineering using parametric interactions, Phys. Rev. Research **2**, 023370 (2020).
[21] D. C. Cole, J. J. Wu, S. D. Erickson, P.-Y. Hou, A. C. Wilson, D. Leibfried, and F. Reiter, Dissipative preparation of W states in trapped ion systems, New J. Phys. **23**, 073001 (2021).
[22] G. Vacanti and A. Beige, Cooling atoms into entangled states, New J. Phys. **11**, 083008 (2009).
[23] F. Reiter, M. J. Kastoryano, and A. S. Sørensen, Driving two atoms in an optical cavity into an entangled steady state using engineered decay, New J. Phys. **14**, 053022 (2012).
[24] M. Malinowski, C. Zhang, V. Negnevitsky, I. Rojkov, F. Reiter, T.-L. Nguyen, M. Stadler, D. Kienzler, K. K. Mehta, and J. P. Home, following Letter, Generation of a Maximally Entangled State Using Collective Optical Pumping, Phys. Rev. Lett. **128**, 080503 (2022).
[25] T. Brown, E. Doucet, D. Ristè, G. Ribeill, K. Cicak, J. Aumentado, R. Simmonds, L. Govia, A. Kamal, and L. Ranzani, Trade off-free entanglement stabilization in a superconducting qutrit-qubit system, arXiv:2107.13579.
[26] R. B. Blakestad, Transport of trapped-ion qubits within a scalable quantum processor, Ph. D. thesis, University of Colorado Boulder, 2010.
[27] C. Langer, R. Ozeri, J. D. Jost, J. Chiaverini, B. DeMarco, A. Ben-Kish, R. B. Blakestad, J. Britton, D. B. Hume, W. M. Itano, D. Leibfried, R. Reichle, T. Rosenband, T. Schaetz, P. O. Schmidt, and D. J. Wineland, Long-Lived Qubit Memory Using Atomic Ions, Phys. Rev. Lett. **95**, 060502 (2005).
[28] B. E. King, C. S. Wood, C. J. Myatt, Q. A. Turchette, D. Leibfried, W. M. Itano, C. Monroe, and D. J. Wineland, Cooling the Collective Motion of Trapped Ions to Initialize a Quantum Register, Phys. Rev. Lett. **81**, 1525 (1998).
[29] D. Leibfried, R. Blatt, C. Monroe, and D. Wineland, Quantum dynamics of single trapped ions, Rev. Mod. Phys. **75**, 281 (2003).
[30] See Supplemental Material at http://link.aps.org/supplemental/10.1103/PhysRevLett.128.080502, which includes Refs. [31–33], for additional information.
[31] J. R. Johansson, P. D. Nation, and F. Nori, QuTiP2: A PYTHON framework for the dynamics of open quantum systems, Comput. Phys. Commun. **184**, 1234 (2013).
[32] D. J. Wineland, M. Barrett, J. Britton, J. Chiaverini, B. DeMarco, W. M. Itano, B. Jelenkovic, C. Langer, D. Leibfried, V. Meyer, T. Rosenband, and T. Schatz, Quantum information processing with trapped ions, Phil. Trans. R. Soc. A **361**, 1349 (2003).
[33] C. W. Chou, D. B. Hume, M. J. Thorpe, D. J. Wineland, and T. Rosenband, Quantum Coherence between Two Atoms Beyond $Q = 10^{15}$, Phys. Rev. Lett. **106**, 160801 (2011).
[34] J. P. Gaebler, T. R. Tan, Y. Lin, Y. Wan, R. Bowler, A. C. Keith, S. Glancy, K. Coakley, E. Knill, D. Leibfried, and D. J. Wineland, High-Fidelity Universal Gate Set for $^{9}Be^{+}$ Ion Qubits, Phys. Rev. Lett. **117**, 060505 (2016).
[35] B. Efron, Better bootstrap confidence intervals, J. Am. Stat. Assoc. **82**, 171 (1987).
[36] R. Ozeri, W. M. Itano, R. B. Blakestad, J. Britton, J. Chiaverini, J. D. Jost, C. Langer, D. Leibfried, R. Reichle, S. Seidelin, J. H. Wesenberg, and D. J. Wineland, Errors in trapped-ion quantum gates due to spontaneous photon scattering, Phys. Rev. A **75**, 042329 (2007).
[37] H. Uys, M. J. Biercuk, A. P. VanDevender, C. Ospelkaus, D. Meiser, R. Ozeri, and J. J. Bollinger, Decoherence due to Elastic Rayleigh Scattering, Phys. Rev. Lett. **105**, 200401 (2010).
[38] D. A. Lidar, I. L. Chuang, and K. B. Whaley, Decoherence-Free Subspaces for Quantum Computation, Phys. Rev. Lett. **81**, 2594 (1998).
[39] L. M. Duan and G. C. Guo, Reducing decoherence in quantum-computer memory with all quantum bits coupling to the same environment, Phys. Rev. A **57**, 737 (1998).
[40] D. Kielpinski, V. Meyer, M. A. Rowe, C. A. Sackett, W. M. Itano, C. Monroe, and D. J. Wineland, A decoherence-free quantum memory using trapped ions, Science **291**, 1013 (2001).
[41] U. Eichmann, J. C. Bergquist, J. J. Bollinger, J. M. Gilligan, W. M. Itano, D. J. Wineland, and M. G. Raizen, Young's Interference Experiment with Light Scattered from Two Atoms, Phys. Rev. Lett. **70**, 2359 (1993).
[42] D. J. Wineland, C. Monroe, W. M. Itano, D. Leibfried, B. E. King, and D. M. Meekhof, Experimental issues in coherent quantum-state manipulation of trapped atomic ions, J. Res. Natl. Inst. Stand. Technol. **103**, 259 (1998).
[43] F. Mintert and C. Wunderlich, Ion-Trap Quantum Logic Using Long-Wavelength Radiation, Phys. Rev. Lett. **87**, 257904 (2001).
[44] C. Ospelkaus, C. E. Langer, J. M. Amini, K. R. Brown, D. Leibfried, and D. J. Wineland, Trapped-Ion Quantum Logic Gates Based on Oscillating Magnetic Fields, Phys. Rev. Lett. **101**, 090502 (2008).

[45] S. Wölk and C. Wunderlich, Quantum dynamics of trapped ions in a dynamic field gradient using dressed states, New J. Phys. **19**, 083021 (2017).

[46] R. Srinivas, S. C. Burd, R. T. Sutherland, A. C. Wilson, D. J. Wineland, D. Leibfried, D. T. C. Allcock, and D. H. Slichter, Trapped-Ion Spin-Motion Coupling with Microwaves and a Near-Motional Oscillating Magnetic Field Gradient, Phys. Rev. Lett. **122**, 163201 (2019).

[47] C. D. Bruzewicz, J. Chiaverini, R. McConnell, and J. M. Sage, Trapped-ion quantum computing: Progress and challenges, Appl. Phys. Rev. **6**, 021314 (2019).